Supplemental Tables

Table S1. Significant frequency clusters for Figure 2B and 2C[a]

Power	Region	Range	Cluster	Sum	97.5%	Shuffle Mean ± STD	p value (≤)	Effect[b] Size
	DG	3-12 Hz	6-12 Hz	4.91	1.92	0.11 ± 0.48	0.000	10.00
	DG	12-90 Hz	13-90 Hz	52.96	14.35	2.80 ± 4.76	0.000	10.54
	CA3	3-12 Hz	7-10 Hz	2.85	1.98	0.18 ± 0.63	0.009	4.24
	CA3	12-90 Hz	15-90 Hz	51.90	14.53	2.67 ± 4.36	0.000	11.29
	CA1	12-90 Hz	25-90 Hz	44.90	10.83	2.39 ± 3.71	0.000	11.46
	SUB	3-12 Hz	6-10 Hz	3.92	1.93	0.15 ± 0.55	0.000	6.85
	SUB	12-90 Hz	45-89 Hz	30.72	11.52	2.60 ± 3.60	0.000	7.81
	Average	3-12 Hz	6-12 Hz	4.85	0.00	0.00 ± 0.06	0.000	80.8
	Interaction	3-12 Hz	7-10 Hz	2.98	2.00	0.08 ± 0.41	0.000	7.07
	Interaction	12-90 Hz	13-90 Hz	53.00	0.00	0.02 ± 0.28	0.000	189.2
Coherence	Regions	Range	Cluster	Sum	97.5%	Shuffle Mean ± STD	p value (≤)	Effect Size
	DG/CA3	12-90 Hz	13-89 Hz	52.82	11.33	2.46 ± 3.74	0.000	13.47
	CA3/CA1	3-12 Hz	7-9 Hz	1.99	1.93	0.09 ± 0.42	0.005	4.52
	CA3/CA1	12-90 Hz	32-50 Hz	12.50	10.76	2.35 ± 3.40	0.016	2.99
	CA1/SUB	3-12 Hz	7-12 Hz	3.96	2.86	0.20 ± 0.67	0.002	5.61
	CA1/SUB	12-90 Hz	13-26 Hz	9.90	8.81	2.14 ± 3.19	0.016	2.43
	Interaction	3-12 Hz	6-12 Hz	5.00	2.75	0.18 ± 0.64	0.000	7.53
	Interaction	12-90 Hz	13-63 Hz	34.84	26.97	3.44 ± 8.07	0.000	3.89

a. Data were evaluated separately for 3-12 Hz vs. 12-90 Hz ranges, and thus a 97.5 percentile criterion was used to evaluate statistical significance of observed cluster sums.
b. Effect size was calculated as a z score of the cluster sum in relation to the average and standard deviation of the shuffle distribution.

Table S2. Significant time clusters for Figure 3B and 3C[a]

Slow Gamma Power	Region	Cluster (s)	Sum	95%	Shuffle Mean ± STD	p value (≤)	Effect[b] Size
	DG	-0.45 to 0.00	9.64	8.69	2.75 ± 3.48	0.036	1.98
	DG	0.30 to 1.80	29.53	8.69	2.75 ± 3.48	0.000	7.70
	CA3	-0.75 to 0.00	15.45	8.61	2.42 ± 3.23	0.002	4.03
	CA3	0.30 to 1.80	29.05	8.61	2.42 ± 3.23	0.000	8.24
	CA1	0.50 to 1.10	11.45	8.59	2.43 ± 3.35	0.018	2.69
Slow Gamma Coherence	**Regions**	**Cluster (s)**	**Sum**	**95%**	**Shuffle Mean ± STD**	**p value (≤)**	**Effect Size**
	DG/CA3	0.60 to 1.80	23.24	8.61	2.40 ± 3.21	0.000	6.49
	CA3/CA1	0.40 to 1.20	15.16	8.32	2.46 ± 3.20	0.003	3.97
	CA3/CA1	1.30 to 1.80	9.49	8.32	2.46 ± 3.20	0.030	2.20
Fast Gamma Power	**Region**	**Cluster (s)**	**Sum**	**95%**	**Shuffle Mean ± STD**	**p value (≤)**	**Effect Size**
	DG	-0.049 to 1.80	36.34	9.34	2.56 ± 3.53	0.000	9.57
	CA3	-0.15 to 1.80	38.60	8.36	2.18 ± 3.20	0.000	11.38
	CA1	-0.049 to 1.30	26.77	8.57	2.13 ± 3.11	0.000	7.92
	SUB	-0.40 to 0.15	11.63	8.92	2.92 ± 3.52	0.017	2.47
	SUB	0.65 to 1.80	22.59	8.92	2.92 ± 3.52	0.001	5.59
Fast Gamma Coherence	**Regions**	**Cluster (s)**	**Sum**	**95%**	**Shuffle Mean ± STD**	**p value (≤)**	**Effect Size**
	CA3/CA1	0.25 to 0.90	13.72	7.73	2.40 ± 3.00	0.002	3.77

a. A 95 percentile criterion was used to evaluate statistical significance of observed cluster sums.
b. Effect size was calculated as a z score of the cluster sum in relation to the average and standard deviation of the shuffle distribution.

Table S3. Percent of Neurons Significantly Phase Modulated by Range and Subregion/Subregion Pair in Figure 4 and Figure S4

Neurons Modulated by Local Field (Related to Figure 4)				
	Theta	Beta	Slow Gamma	Fast Gamma
DG/DG[a]	79% (54/68)[b]	48% (30/62)	57% (33/58)	28% (16/57)
CA3/CA3	40% (72/180)	26% (57/216)	27% (58/213)	38% (81/215)
CA1/CA1	51% (142/280)	29% (88/308)	13% (38/289)	15% (45/300)
SUB/SUB	67% (29/43)	36% (16/45)	22% (10/46)	32% (14/44)

Neurons Modulated by Downstream Field (Related to Figure S4)				
	Theta	Beta	Slow Gamma	Fast Gamma
DG/CA3	64% (38/59)	67% (39/58)	70% (37/53)	60% (33/55)
CA3/CA1	52% (95/184)	22% (43/193)	18% (34/187	23% (42/183)
CA1/SUB	79% (262/333)	23% (74/328)	9% (29/307)	10% (31/296)

a. The first subregion in the pair indicates which subregion's spikes were being considered while the second subregion listed indicates the subregion from which the local field potential was drawn. E.g., "CA3/CA1" indicates CA3 spiking was being compared to oscillations recorded from CA1.

b. Values are presented as the percent of total neurons recorded that were significantly modulated by oscillatory phase. The raw number of significantly modulated neurons and the total number of neurons recorded are in parentheses.

Table S4. Significant frequency clusters for Figure 6A[a]

Power	Region	Range	Cluster	Sum	97.5%	Shuffle Mean ± STD	p value (≤)	Effect[c] Size
	DG	12-90 Hz	26-59 Hz	22.72	10.43	2.28 ± 3.27	0.000	6.25
	CA3	12-90 Hz	25-51 Hz	18.56	10.74	2.32 ± 3.43	0.002	4.73
	Average	12-90 Hz	25-59 Hz	23.47	0[b]	0 ± 0	0.000	Inf[d]
	Interaction	12-90 Hz	32-50 Hz	12.75	5.50	0.34 ± 2.17	0.000	5.72

a. Data were evaluated separately for 3-12 Hz vs. 12-90 Hz ranges, and thus a 97.5 percentile criterion was used to evaluate statistical significance of observed cluster sums.

b. A value of 0 for the 97.5% criterion indicates that no randomly-generated clusters surpassed the initial cluster threshold (see Experimental Procedures for details)

c. Effect size was calculated as a z score of the cluster sum in relation to the average and standard deviation of the shuffle distribution.

d. A value of infinity is possible when no randomly-generated clusters surpassed the initial cluster threshold, and therefore the average and standard deviation for the shuffle distribution are equal to zero.

Table S5. Statistics for Bar Graphs in Figure 6C (Power), 6D (Coherence), and 6E (DTF)

		One-Way RM ANOVA			Linear Trend		
Slow Gamma		F (2,10)	p	partial η^2	F (1,5)	p	partial η^2
	Power						
	DG	14.353	0.001	0.742	28.458	0.003	0.851
	CA3	12.935	0.002	0.721	16.794	0.009	0.771
	CA1	2.177	0.164	0.303	2.497	0.175	0.333
	SUB	0.829	0.464	0.142	4.193	0.096	0.456
	Average	11.662	0.002	0.700	15.583	0.011	0.757
	Coherence						
	DG/CA3	0.995	0.404	0.166	2.251	0.194	0.310
	CA3/CA1	0.666	0.535	0.118	0.007	0.983	0.001
	CA1/SUB	3.393	0.075	0.404	6.994	0.046	0.583
	Average	2.842	0.105	0.362	11.851	0.018	0.703
	DTF						
	DG/CA3	4.145	0.049	0.453	8.010	0.037	0.616
	CA3/CA1	2.170	0.165	0.303	2.274	0.192	0.313
	CA1/SUB	0.390	0.687	0.072	0.622	0.466	0.111
	Average	9.088	0.006	0.645	19.348	0.007	0.795
Fast Gamma		F (2,10)	p	partial η^2	F (1,5)	p	partial η^2
	Power						
	DG	4.012	0.053	0.445	4.775	0.081	0.489
	CA3	3.186	0.085	0.389	3.595	0.116	0.418
	CA1	1.184	0.345	0.192	1.086	0.345	0.178
	SUB	0.340	0.720	0.064	0.293	0.611	0.055
	Average	1.983	0.188	0.284	2.010	0.215	0.287
	Coherence						
	DG/CA3	0.278	0.763	0.053	0.079	0.790	0.016
	CA3/CA1	0.098	0.908	0.19	0.097	0.769	0.019
	CA1/SUB	0.110	0.897	0.021	0.035	0.858	0.007
	Average	0.053	0.949	0.010	0.068	0.804	0.013
	DTF						
	DG/CA3	0.849	0.456	0.145	0.538	0.496	0.097
	CA3/CA1	0.607	0.564	0.108	0.627	0.464	0.111
	CA1/SUB	0.631	0.552	0.112	0.752	0.426	0.131
	Average	0.406	0.677	0.075	0.003	0.959	0.001

Table S6. Significant frequency clusters for Figure 7A and 7B[a]

Power	Region	Range	Cluster	Sum	97.5%	Shuffle Mean ± STD	p value (≤)	Effect[c] Size
	Average	12-90 Hz	28-40 Hz	8.66	0[b]	0.00 ± 0.00	0.000	Inf[d]
	Interaction	12-90 Hz	67-75 Hz	5.65	0[b]	0.01 ± 0.22	0.000	25.64
Coherence	Regions	Range	Cluster	Sum	97.5%	Shuffle Mean ± STD	p value (≤)	Effect Size
	CA1/SUB	12-90 Hz	26-41 Hz	10.27	8.74	1.92 ± 2.84	0.010	2.94

a. Data were evaluated separately for 3-12 Hz vs. 12-90 Hz ranges, and thus a 97.5 percentile criterion was used to evaluate statistical significance of observed cluster sums.
b. A value of 0 for the 97.5% criterion indicates that no randomly-generated clusters surpassed the initial cluster threshold of (see Experimental Procedures for details).
c. Effect size was calculated as a z score of the cluster sum in relation to the average and standard deviation of the shuffle distribution.
d. A value of infinity is possible when no randomly-generated clusters surpassed the initial cluster threshold, and therefore the average and standard deviation for the shuffle distribution are equal to zero.

Table S7. Statistics for Bar Graphs in Figure 7C (Power), 7D (Coherence), and 7E (DTF)

		One-Way RM ANOVA			Linear Trend		
Slow Gamma		F (2,10)	p	partial η^2	F (1,5)	p	partial η^2
	Power						
	DG	4.521	0.040	0.475	11.639	0.019	0.699
	CA3	3.725	0.062	0.427	6.835	0.047	0.578
	CA1	1.581	0.253	0.240	1.651	0.255	0.248
	SUB	1.025	0.394	0.170	3.858	0.107	0.436
	Average	3.504	0.070	0.412	6.835	0.047	0.578
	Coherence						
	DG/CA3	5.138	0.029	0.507	40.294	0.001	0.890
	CA3/CA1	0.348	0.715	0.065	0.398	0.556	0.074
	CA1/SUB	4.611	0.038	0.480	5.672	0.063	0.531
	Average	5.330	0.027	0.516	14.410	0.013	0.742
	DTF						
	DG/CA3	1.869	0.204	0.272	3.038	0.142	0.378
	CA3/CA1	0.438	0.657	0.080	0.061	0.815	0.12
	CA1/SUB	0.812	0.471	0.140	0.610	0.470	0.109
	Average	1.759	0.222	0.260	2.709	0.161	0.351
Fast Gamma		F (2,10)	p	partial η^2	F (1,5)	p	partial η^2
	Power						
	DG	2.970	0.097	0.373	0.437	0.538	0.080
	CA3	1.045	0.387	0.173	1.281	0.309	0.204
	CA1	1.821	0.212	0.267	1.870	0.280	0.272
	SUB	1.285	0.319	0.204	1.265	0.312	0.202
	Average	1.043	0.388	0.173	0.337	0.587	0.063
	Coherence						
	DG/CA3	0.931	0.426	0.157	0.236	0.647	0.045
	CA3/CA1	3.894	0.056	0.438	15.981	0.010	0.762
	CA1/SUB	1.109	0.369	0.181	0.783	0.417	0.135
	Average	1.548	0.260	0.236	0.984	0.367	0.164
	DTF						
	DG/CA3	0.190	0.830	0.037	0.013	0.915	0.002
	CA3/CA1	0.321	0.733	0.060	0.012	0.917	0.002
	CA1/SUB	1.274	0.321	0.203	0.628	0.464	0.112
	Average	0.189	0.830	0.036	0.016	0.904	0.003

Supplemental Figures and Legends

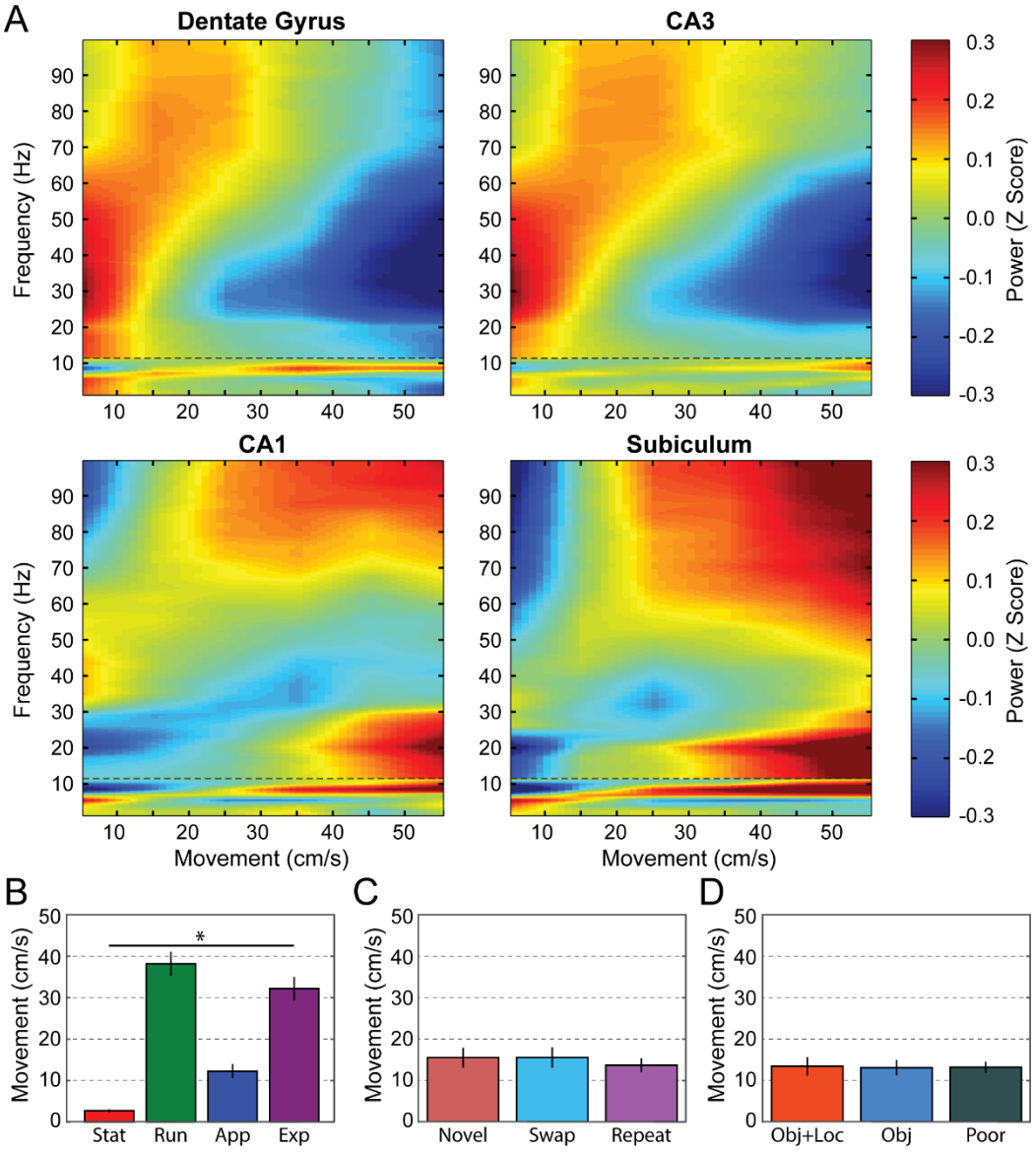

Figure S1, Related to Figure 2. (A). Spectral power differed by subregion and speed of locomotion. Power is shown for each subregion across a broad range of frequencies (1-100 Hz) and speeds of movement (5-55 cm/s). Power is z scored across speed bins within each frequency bin. A dotted line at 12 Hz is shown to indicate that separate taper parameters were employed for >= 12 Hz and for <= 12 Hz. The results for CA3 and CA1 were similar to those presented previously (Ahmed & Mehta, 2012; Kemere et al., 2013; Zheng et al., 2015). Apparent here is the strong degree of similarity between DG and CA3, and between CA1 and subiculum with regards to variation in spectral power by speed of locomotion. **(B).** Average speed of movement was significantly different ($p<0.001$) across behavioral states (S = Stationary; R = Run; E = Exploration; A = Approach). **(C).** Average speed of movement during exploration of objects on lap 3 did not statistically significantly ($p. > .05$) differ by object condition. Speed of movement was averaged across the neural analysis window. **(D)**. Average speed of movement during exploration of novel objects on lap 1 did not statistically significantly ($p. > .05$) differ by memory condition. Speed of movement was averaged across the neural analysis window. Error bars show SEM throughout the figure.

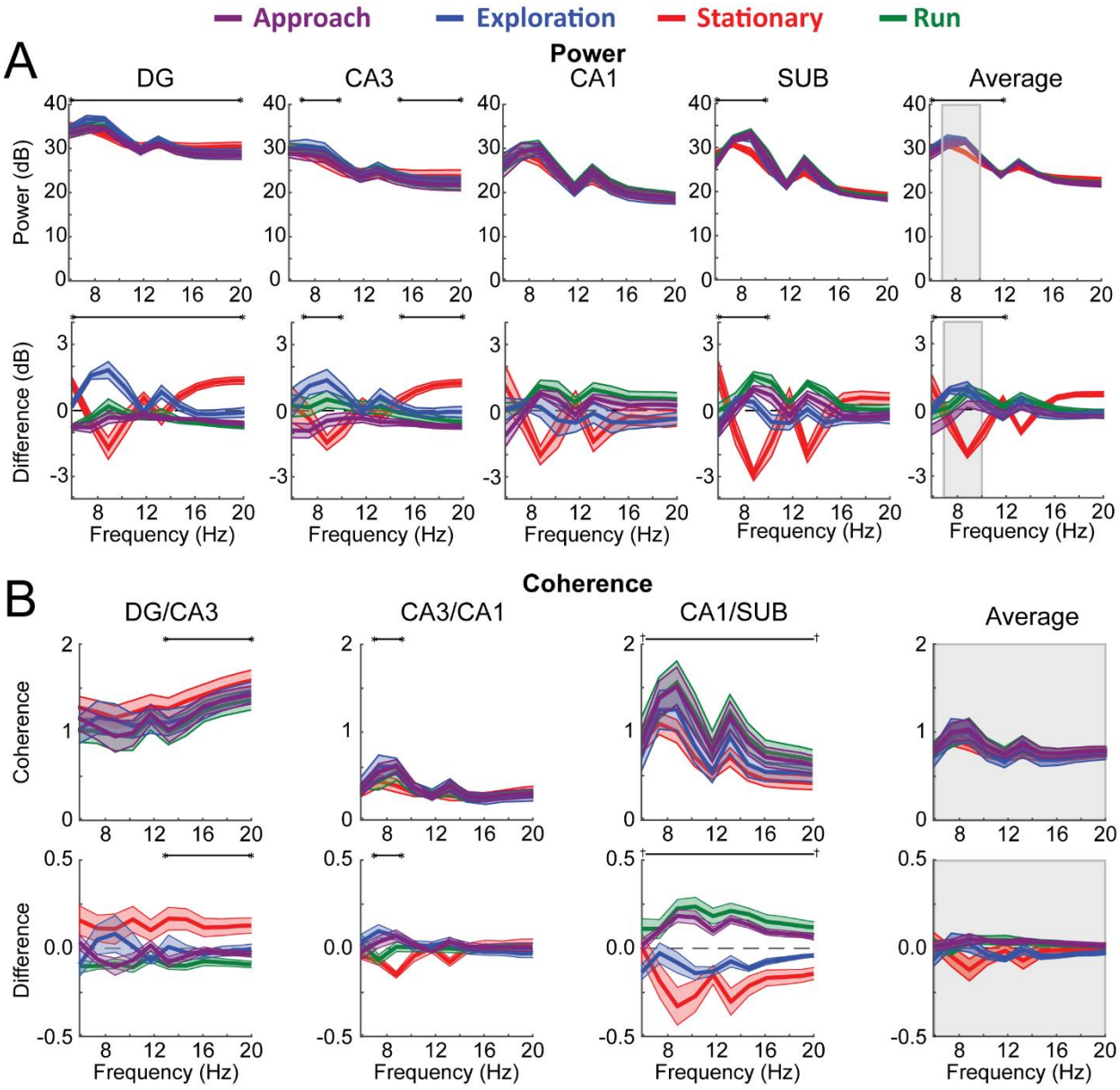

Figure S2, Related to Figure 2. Each subplot presents data identical to that presented in Figure 2, but expanded from 6-20 Hz to visually emphasize differences present in this lower frequency range. (A) Spectral power from 6-20 Hz is shown across the four behavioral states under consideration [i.e., Approach (Purple), Exploration (Blue), Stationary (Red), and Run (Green)]. Frequency clusters that differ significantly across the four behavioral states within each subregion, and with regards to power averaged across subregions, are indicated by bars above each panel bookended by asterisks. Statistical details for each cluster can be seen in Table S1. A significant interaction across behavioral states and subregions is indicated by the gray box presented over the Average hippocampal power subplot (far right). All significant differences presented in this panel, indicated with black lines bookended by asterisks, withstood a Bonferonni alpha correction of 0.05/5, with the denominator chosen based on the number of subregions analyzed plus one for the average across subregions. (B) Coherence from 6-20 Hz is shown for each pair of directly connected subregions, as well as for the average across subregion pairs. Significant differences are indicated as in A, however, here, significant differences are also present that did not withstand a Bonferonni alpha correction of 0.05/4 (for 3 subregion pairs plus the average across pairs). These differences are indicated by black

lines bookended by the dagger symbol (†).

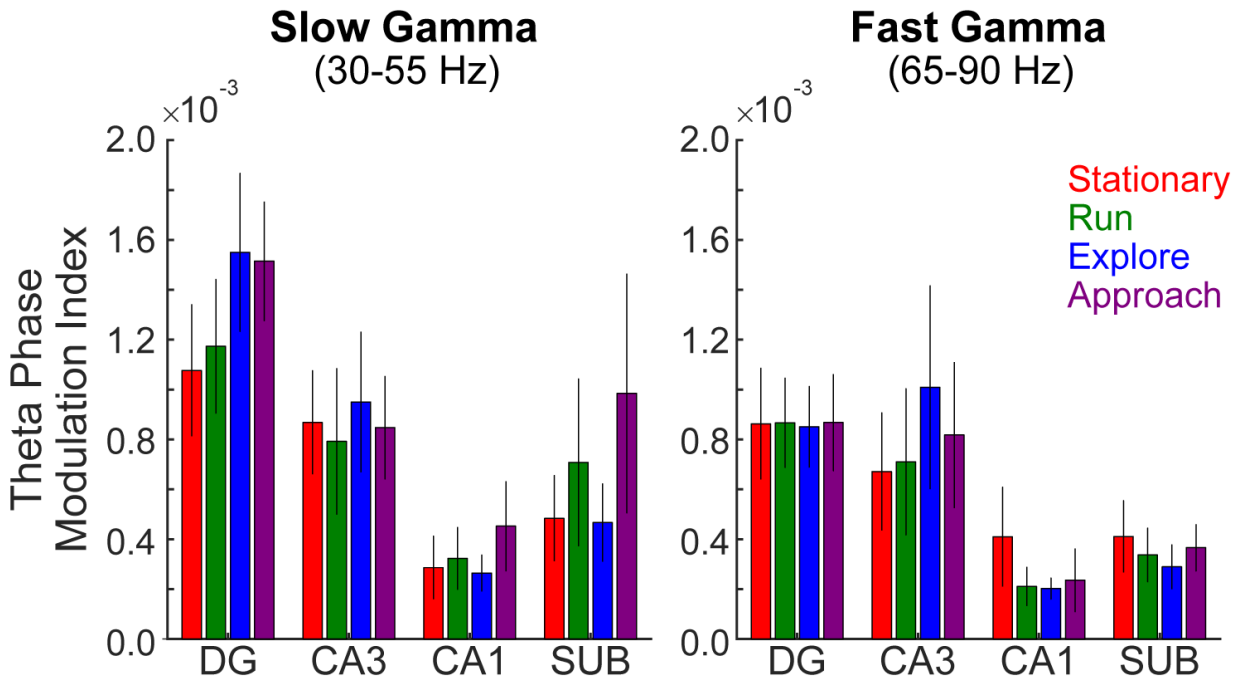

Figure S3. Related to Figure 2. Mean theta-phase modulation index of slow gamma (left panel) and fast gamma (right panel) amplitude. The data are shown for each behavioral state (stationary, run, explore, and approach) for each hippocampal region. Modulation indices were similar across behavioral states (see text). Error bars reflect standard error of the mean across rats (n=6).

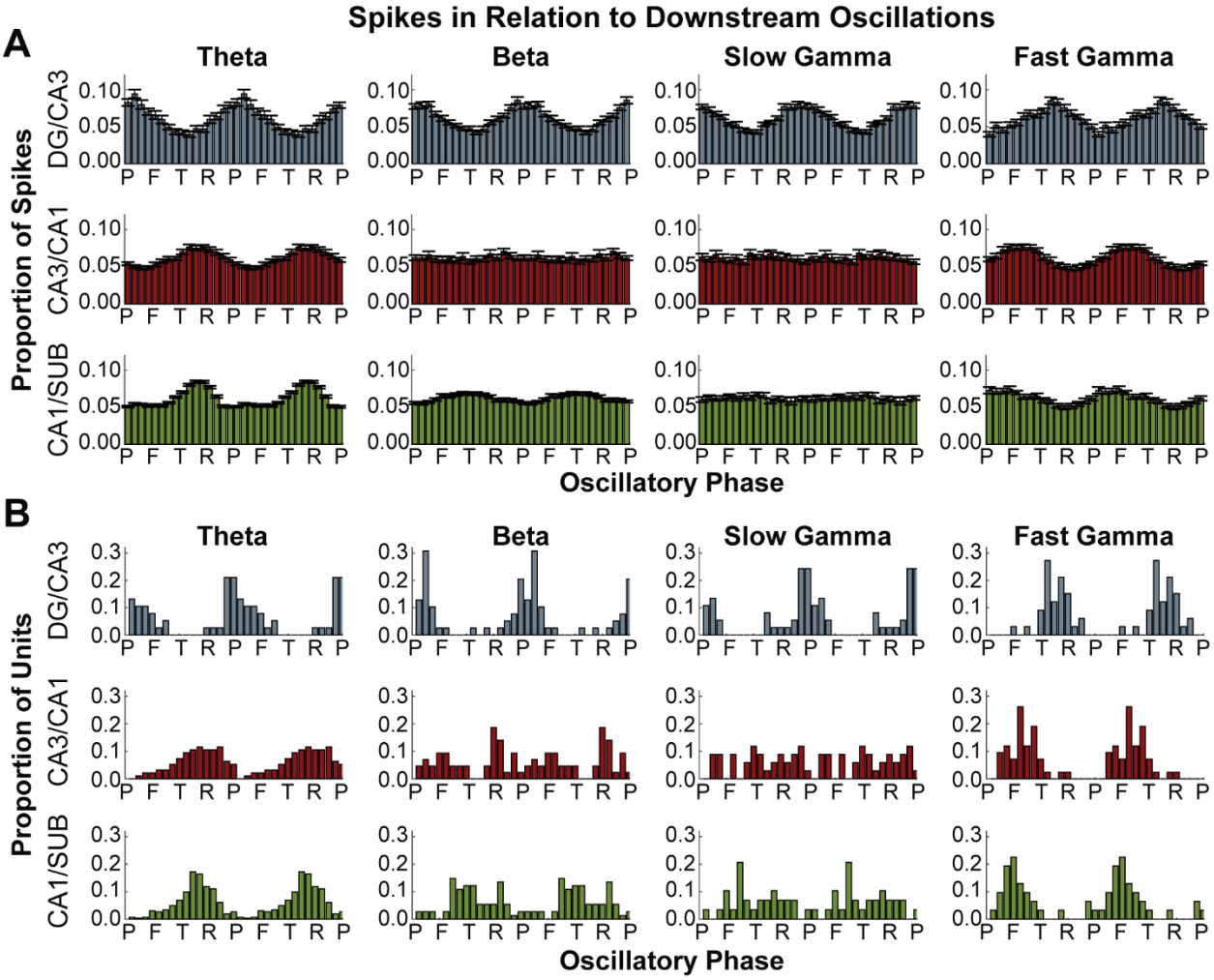

Figure S4, Related to Figure 4. (A) Plotted are the average distributions of action potentials in each subregion relative to the phase (P = peak; F = falling; T = trough; R = rising) of distinct oscillatory rhythms (denoted at top) recorded from the downstream subregion (e.g., the DG/CA3 plot for theta refers to DG spikes in relation to CA3 theta). Averages and error (SEM) are across all neurons found to be significantly phase modulated ($p < 0.05$, Rayleigh's Test). See Table S3 for the percent of neurons by subregion found to be significantly phase modulated. Spiking in relation to each rhythm was only considered when that rhythm was strong (see Methods) and therefore, these graphs do not necessarily represent the same action potentials, nor the same sample of neurons. The finding that many neurons from each subregion aligned their spiking to these rhythms implies that spikes from upstream regions are able to impact oscillatory activity downstream. Note that the data is plotted twice, replicated across the oscillatory cycle, to aid visualization of periodicity. **(B)** Shown are the distributions across significantly phase modulated neurons of average preferred oscillatory phase for spiking. Note the consistency of preferred phase for neurons in some subregions in relation to distinct rhythms (e.g., subicular neurons and spikes in relation to theta) relative to the lack of a consistent phase preference for other subregions (e.g., CA1 spikes to SUB slow gamma oscillations). As with B, all data is plotted twice across the x axis for visualizing periodicity.

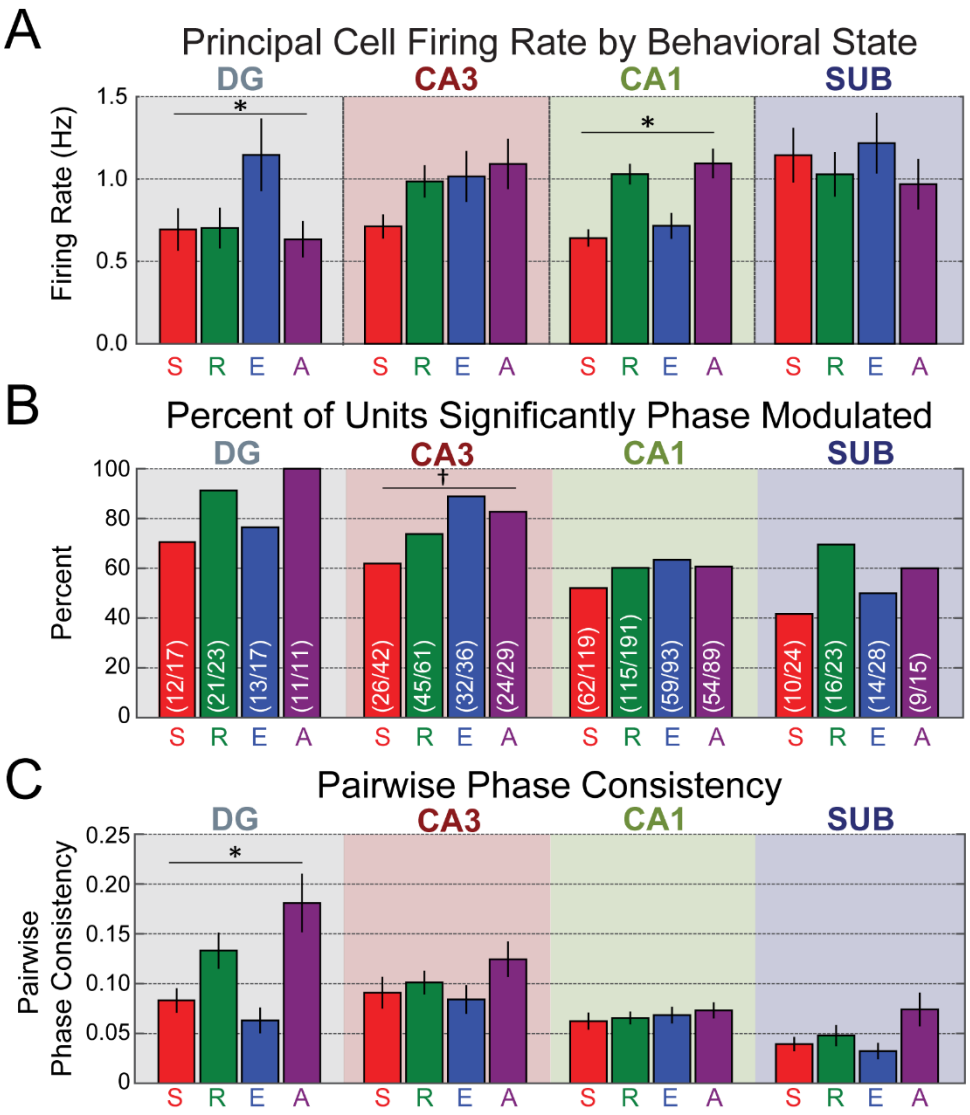

Figure S5. Related to Figure 4. (A) Average firing rate by subregion for each behavioral state (S = Stationary; R = Run; E = Exploration; A = Approach). Error bars reflect standard error of the mean across neurons. After alpha correction, firing rate differed significantly only for CA1 ($p = <0.0001$), reflected by firing rates most elevated during locomotive states (Approach and Run) relative to non-locomotive states (Exploration and Stationary), and DG ($p = 0.006$) whose firing rate was greatest during object exploration. **(B).** Principal cell firing aligned strongly with theta recorded from CA1. Bars reflect the percent of significantly phase modulated neurons out of total number of neurons for each behavioral state (S = Stationary; R = Run; E = Exploration; A = Approach) and each subregion DG, CA3, CA1, and SUB (subiculum)]. The percent of neurons did not differ significantly for any region after Bonferonni alpha correction for four subregions (DG: $p = 0.114$; CA3: $p = 0.035$; CA1: $p = 0.345$; SUB, $p = 0.250$). Percentages reflected by all bars presented were significantly greater than chance (~5%) as tested with a random permutation approach in which the actual percent of neurons statistically modulated by phase were compared to the percentages attained from 1000 shuffles where the number of spikes and neurons remains constant, but spike phases were randomly drawn from a circular uniform distribution. **(C)** Pairwise Phase Consistency for the neurons recorded from each subregion divided by behavioral state. In DG, pairwise phase consistency differed significantly across conditions such that the most elevated levels were observed for locomotive relative to non-locomotive states ($p < 0.001$). More detailed statistics are presented the Results and Discussion section.

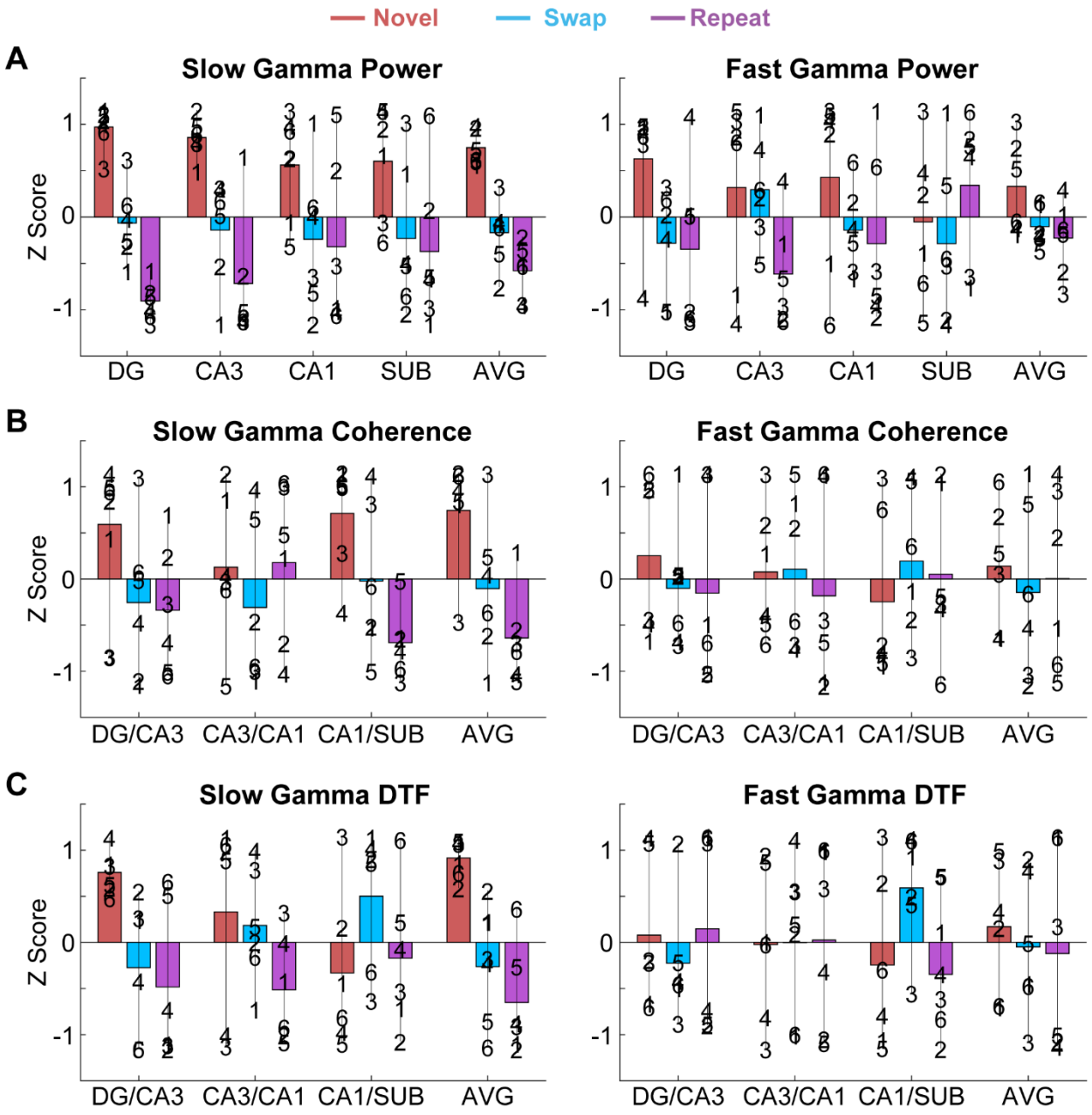

Figure S6, Related to Figure 6. The data from Figure 6, showing spectral measures during the first 1 s of object exploration on lap 3 split by object condition, is reproduced here but with each rat's data represented by an identifying number for better visualization of variability across rats. Data was z-scored to account for magnitude differences with increasing frequency due to spectral power exhibiting a 1/f distribution, and for improved visualization of effect magnitude. (A) Z scored slow gamma and fast gamma power for each subregion and for the average across subregions. (B) Z scored slow gamma and fast gamma coherence between each pair of directly connected subregions and averaged across subregion pairs. (C) Z scored slow gamma and fast gamma directed transfer function (DTF). For statistical information, see significance markers in Figure 6 and statistical details presented in Table S5.

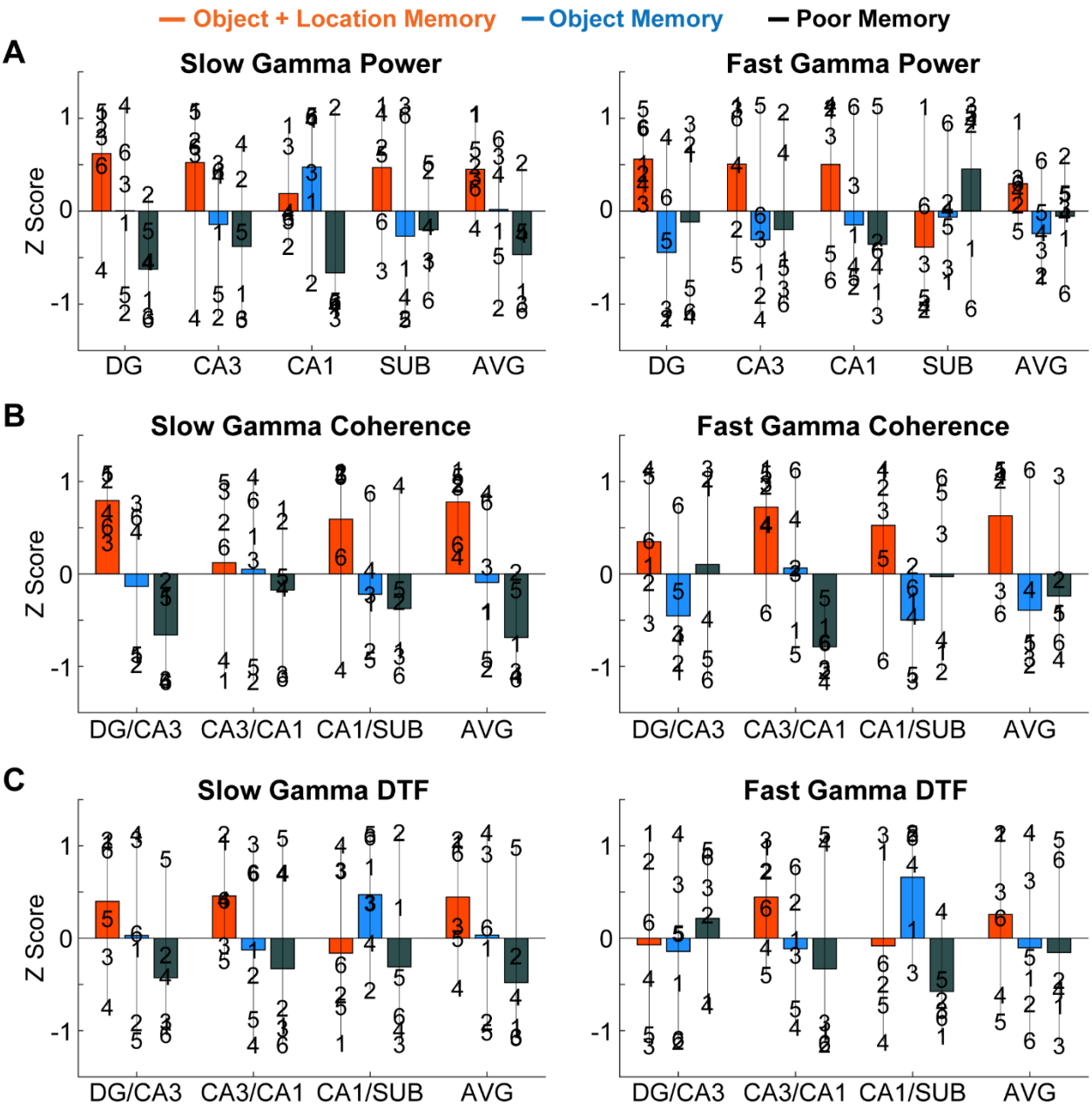

Figure S7, Related to Figure 7. The data from Figure 7, showing spectral measures during the first 1.5 s of object exploration on lap 1 split by subsequent memory, is reproduced here but with each rat's data represented by an identifying number for better visualization of variability across rats. (A) Z scored slow gamma and fast gamma power for each subregion and for the average across subregions. (B) Z scored slow gamma and fast gamma coherence between each pair of directly connected subregions and averaged across subregion pairs. (C) Z scored slow gamma and fast gamma directed transfer function (DTF). For statistical information, see significance markers in Figure 7 and statistical details presented in Table S7.

Supplemental Experimental Procedures

Behavioral Training

The behavioral task required rats to run consecutive clockwise laps around an elevated circular track (diameter = 91.5cm/ track width = 7 cm) for small chocolate sprinkle rewards at the completion of each lap. Rats were trained daily to perform these laps up to criteria (80 laps in 40 minutes), a process lasting approximately five weeks. Throughout the training process, rats were additionally habituated to touching of their heads in anticipation of the neural recording experiments. After surgical implantation of a chronic neural recording assembly (see below), rats were re-trained daily up to criteria, at which point performance was maintained with approximately twice-weekly training sessions until recording tetrodes were in position. One day before initial testing, rats were exposed to objects placed on retractable flaps adhered to the perimeter of the elevated track for the purpose of reducing potential neophobia at test related to rats never having encountered any objects before along the track.

During recognition memory testing (see Figure 5 and main text), the degree of exploration of objects was at the rats' discretion, relying on rats' innate curiosity and preference for novelty, and never rewarded, encouraged, or otherwise manipulated by experimenters. When objects were repeated from a prior lap, duplicates were employed to avoid scent marking. The memory conditions assigned to each trial alternated in a 2:1 fashion, such that there were two Swap trials for every one Repeat/Novel trial. The locations for the Repeat and Novel objects were counter-balanced across trials. The number of trials and test sessions conducted in any single day was limited by the quality of recordings and rat performance (i.e., willingness to explore objects at study on lap 1).

Objects

Example objects can be seen in Figure 5. Objects were randomly pulled from a set of approximately 320 unique objects, with up to four duplicates of each unique object. All objects were purchased from a local store to be used solely for object recognition memory testing with rats in our laboratory. Objects ranged in size from approximately 7 x 7 x 7 cm to 17 x 17 x 10 cm. Object size was equated within trials to control for exploration time effects related to this factor. Objects were randomly assigned to experimental conditions. All objects were novel to rats at the beginning of testing, and were washed immediately after testing, with all duplicates of that object, to limit scent marking and ensure all duplicates of the same objects were handled similarly. Objects were adhered to retractable flaps on the outside of the elevated circular track using Velcro.

Surgical Procedure

Sterile-tip stereotaxic surgery was performed after rats were deeply anesthetized with isoflurane (1–3% in oxygen) and given buprenorphine (0.05 mg/kg) as an analgesic. Rats were implanted with a custom chronic electrophysiological recording headstage that contained up to 32 independently movable tetrodes. Tetrodes were funneled through two stainless steel cannulae (14 gauge and 17 gauge) to concentrate their positioning over the hippocampal subregions of interest—DG, CA3, CA1, and subiculum. Craniotomies spanned an area from approximately 2.6 to 6.4 mm posterior to bregma and 1.3 to 4.2 mm lateral to the central suture, with tetrodes typically falling within 3 to 6 mm posterior to bregma and 1.8 to 3.8 mm lateral to the central suture. Each tetrode consisted of four 12.5 μm nichrome wires whose tips were plated with gold to reduce the impedance to 200 kΩ at 1 kHz. Rats were monitored in the lab for several hours after surgery, and daily for the following three days. Additional doses of buprenorphine (0.05 mg/kg) were given immediately after surgery and the following morning. Meloxicam (Metacam) was administered immediately after surgery (0.75ml) and each of the two following mornings for pain relief.

Neural Data Acquisition

Following a one-week recovery period, tetrodes were gradually lowered over the course of 1-3 months to the pyramidal layers of CA3, CA1, and subiculum and the granule cell layer of DG occurred over several weeks and was assisted by known electrophysiological hallmarks [e.g., dentate spikes (Bragin et al., 1995), sharp-wave ripples (Buzsaki., 1986)]. A stainless steel screw implanted in the skull above the cerebellum served as the reference for LFPs during recording, whereas a tetrode within the hippocampus but without single units served as the reference for spike channels. Neural data were acquired using NSpike data acquisition system (nspike.sourceforge.net). Tetrodes were never turned prior to testing on days in which experiments were performed, though minor adjustments were made after test sessions to maintain good single unit isolation for the following days.

For LFP analyses in CA3, CA1, and subiculum, one tetrode in the middle third of each region's transverse axis (proximal to distal relative to DG) was selected for each rat. This intermediate portion along the proximal/distal axis was selected because the intermediate portion of CA3 projects directly to the intermediate portion in CA1 which projects to the intermediate portion of subiculum, and because this portion of each of the regions receives input from both lateral and medial entorhinal cortex (Witter and Amaral, 2004). The intermediate portion of DG was not selectively targeted as dentate cells project to the entire transverse extent of CA3 (Swanson et al., 1978; Gaarskjaer, 1986).

Statistical Reporting Format

Unless otherwise noted, all figures and central tendency reporting is provided as mean plus and minus the standard error of the mean.

Behavioral Coding.

Experimental videos were scored using custom written software. A behavioral flag was assigned to each event of interest (e.g., lap start and end times, object exploration initiation and offset). Rats were considered to be exploring objects only when their noses were within approximately 1 cm of the object and rats were exhibiting signs of active investigation. Exploration events including excessive chewing were discarded and data for that trial were not used. For analyses of rat locomotion, rats' positions were tracked within the videos in Cartesian coordinates using custom written software in MATLAB (Mathworks) which detected the centroid of two LEDs affixed to the recording headstage on rats' heads. The frame rate of the video was 30 frames per second.

We separated rats' activity on blank laps into periods of time in which the rat was not locomoting (Stationary) and periods of time in which the rats were locomoting (Run). To accomplish this task, spatial coordinate data (see above) and LFP data on blank laps were divided into 250 ms segments. Stationary bouts were defined as 8 consecutive 250 ms segments in which rats moved less than 10 cm/s. Run bouts were defined as 8 consecutive 250 ms segments in which rats moved more than 10 cm/s. A threshold of 10 cm/s, rather than 0 cm/s, was chosen to allow for small head movements and rearing in the Stationary condition. Exploration bouts were defined as period of time lasting at least 2 s in which rats were consistently engaging in active investigation of novel objects, while Approach bouts were defined as the 2s of time immediately preceding exploration onset.

Analyses of Neural Data.

Power and Coherence. All data analyses were performed using custom written code in MATLAB (Mathworks). Spectral analyses implemented a multitaper fast Fourier transform method for calculating coherence and power (Bokil et al., 2010). Spectral power, also referred to as spectrum or auto-spectra, is a metric providing information about the prevalence of oscillatory activity at each frequency within a LFP sweep. Power was calculated as the product of the complex Fourier coefficients multiplied by their complex conjugate. Power was log-transformed to account for a 1/frequency distribution, and converted from bels to decibels by multiplying log transformed values by ten. Coherence is a metric for covariance of phase and amplitude between two LFPs. It was calculated as the absolute magnitude of coherency, which is cross spectrum normalized by the product of the two auto-spectra (i.e., power for each LFP). Coherence was Fisher transformed to stabilize variance at the tails of the distribution, thus explaining why values greater than 1 were observed when coherence was particularly high. Unless noted otherwise, sliding 0.5 s windows with step size of 0.05 s were used to calculate spectral estimates to reduce the possible complication of nonstationarity in the data (Mitra and Pesaran, 1999). To ensure adequate spectral resolution within each frequency range of interest, multitaper FFTs employed separate taper parameters for the theta range and below (1 – 13 Hz) relative to 13 Hz and above (13 – 90 Hz). For 1 – 13 Hz, we used a frequency half bandwidth of 1 Hz (-1 Hz to +1 Hz) and a single taper for each 0.5 s section of data. For 13 Hz and above, we used a frequency half bandwidth of 6 Hz (-6 Hz to +6 Hz), enabling the use of five well-concentrated orthogonal tapers for each 0.5 s section of data. To account for possible bias in spectral metric calculation, in cases where an uneven number of trials were present across conditions within a rat, a subsampling procedure where trials for each condition were subsampled down to the lowest number of trials present across conditions was performed. Subsampling was repeated 1,000 times, or the max allowable number of times when the max number of unique subsamples was less than 1,000. The final values for each condition were then calculated by averaging across these subsampling iterations.

Directed Transfer Function. Non-normalized directed transfer function, also referred to as the transfer matrix (H), is the inverse of the fast Fourier transformed multivariate autoregressive coefficient matrix. Non-normalized directed transfer function is an autoregressive metric that assesses the ability of the past history of time series X, back to a specified lag (model order), to predict the current state of time series Y (Kaminski & Blinowska, 1991). Non-normalized directed transfer function can be considered a form of multivariate Granger causality in the frequency domain. Units are arbitrary. Prior to calculation, LFP amplitudes were z scored within subregion to equate amplitude variability across subregions. As with the multitaper approach described above, different parameter sets were employed for 13 Hz and below relative to greater than 13 Hz to improve spectral and temporal resolution. For 5-13 Hz, LFP traces were downsampled by a factor of 14, adjusting the sampling rate to 107.14 Hz. This downsampling factor was chosen as the highest number possible that would still prevent aliasing, allowing for at least eight data points per cycle in the highest frequency under consideration within this range of interest (5 – 13 Hz) [e.g., with 1500 Hz sampling rate, requiring 8 data points per cycle from a 13 Hz oscillation requires at least 1500 Hz / (13 Hz * 8 points) data points (107.14) per second]. A model order of 20 was chosen to accompany at least 1

complete cycle of a 6 Hz theta oscillation. For the higher frequency range, from 14-90 Hz, data was downsampled by a factor of 2 adjusting the sampling rate to 750 Hz allowing for at least 8 data points per cycle of a 90 Hz oscillation. A model order of 30 was chosen, allowing for at least one complete cycle of a 25 Hz oscillation within the specified lag. Model parameters were validated a priori on a subset of the data by verifying whiteness of the noise coefficients, weak correlation among the residuals, stability/stationarity of the model, and consistency of the model. Model validation was performed using the SIFT toolbox (Delorme et al., 2011; Mullen, 2014), implemented through EEGlab (Delorme & Makeig, 2004), and following the suggestions of Ding et al., 2000.

Statistical testing of frequency clusters. A cluster-based permutation approach adapted from (Maris et al., 2007; Maris & Oostenveld, 2007) for more than a single independent variable and more than two levels of each variable was employed. A description of the procedure is as follows. For each frequency bin, an F ratio was calculated. For questions regarding interactions between subregion/subregion pairing and condition, the F ratio was calculated with a two-way repeated measures analysis of variance (ANOVA) with subregion/subregion pairing as one factor and object condition as a second factor. For questions regarding an effect of condition *within* subregion/subregion pairing, a one-way ANOVA was employed with condition as the sole factor. This procedure produced a vector of F values spanning all frequency bins under consideration. To identify potentially-significant frequency clusters, F ratios were next converted to p values corresponding to the lower tail of the F distribution. Thus, higher p values here indicated a lower statistical probability of occurrence (so as to facilitate the cluster-summing procedure described below). This procedure produced a vector of p values spanning all frequency bins under consideration. All p values greater than 0.90 (upper 10^{th} percentile) were then identified as potential clusters and only consecutive groups of those p values of at least a pre-defined length were further considered (two consecutive points for below 13 Hz, four consecutive points for above 13 Hz). The choice of initial cluster detection threshold ($p = 0.90$) is arbitrary but is necessary to identify potential clusters. Separate cluster length criteria were used for the lower and higher frequency ranges as number of frequency bins differed greatly between the two ranges, with far less available in the low frequency range (<= 13 Hz). P values within each identified cluster of points were summed, such that a single sum was recorded for each cluster of sufficient length. These cluster sums recorded from the nonrandomized data were then compared to the maximum cluster sums recorded from each of 1,000 randomizations. This comparison against a random distribution essentially asks: is the difference across conditions present within this particular frequency range greater than the difference that might be observed by chance? When looking for significant differences across conditions within a subregion/subregion pairing, conditions were randomized within rats. When looking for significant interactions between subregion/subregion pairing and condition, both subregion/subregion pairing and condition were randomized within rats. Just as with the non-randomized data, cluster sums were identified in the averages across rats. Cluster sums from the non-randomized data greater than the 97.5^{th} percentile for the randomized cluster sums were denoted as significant. A cutoff of 97.5 was used, rather than 95, as clusters from two separate frequency ranges were statistically evaluated (3-13 Hz and 13-90 Hz).

Spiking Analyses

Across rats and sessions, we recorded 114, 459, 437, and 121 well isolated neurons from DG, CA3, CA1, and subiculum, respectively. Putative interneurons were distinguished from these principal cells based on spike-waveforms, autocorrelograms, and firing rates greater than 4 Hz, a cutoff based on both firing rate distributions from the current data and prior reports (e.g., Anderson & O'Mara, 2003; Mizuseki et al., 2012; Ranck, 1973; Skaggs et al., 1996). Principal cell counts were 104, 448, 424, and 59 from DG, CA3, CA1, and subiculum. For comparisons of firing rates across conditions, units were excluded from consideration if they did not emit at least 50 spikes across all conditions. Significant phase modulation of spiking was said to be present for a given neuron if a Rayleigh's Z-Test for circular non-uniformity returned a p-value of less than 0.05. To evaluate whether or not the percent of neurons significantly modulated by phase differed from the percent expected by chance, the actual percent of significantly modulated neurons was compared to the percentages attained from 1,000 shuffles, where, in each of the shuffles, the number of neurons and action potentials was held constant, but spike phase was randomly drawn from a uniform circular distribution.

When assessing spike-phase relationships with nonstationary rhythms (e.g., beta, slow gamma, fast gamma), only spikes occurring when these oscillations are prominent can be considered, as failure to pre-select periods of strong oscillatory activity can lead to spurious detection of spike-phase relationships (Colgin et al., 2009). Thus, when assessing spike-phase relationships to frequency ranges above theta, which is consistently strong throughout the rat hippocampus, we filtered each LFP in the frequency range of interest, then extracted an amplitude envelope for the LFP via a Hilbert transform and detected periods of time in which beta and gamma rhythms were strong for further consideration. We defined oscillatory events as time points in which the amplitude envelope surpassed an edge threshold of at least 1 standard deviation above average and a peak of at least 1.5 standard

deviations above average. Oscillatory events were required to be at least three cycle lengths long, with the cycle length defined by the average frequency for that range. For example, when looking for events in the slow gamma range (30-55 Hz), detected events were required to last at least 70.587 ms in duration, or three full cycles of a 42.5 Hz rhythm, the average frequency of a slow gamma oscillation. Events occurring within 3 average cycle lengths of one another were considered to be the same event.

Spike-phase alignment to the hippocampal theta rhythm by behavioral state (Figure S5) was assessed in relation to theta recorded from the pyramidal layer of CA1, rather than in relation to each subregion's local theta oscillation. The theta oscillation is largely coherent throughout the hippocampus but most readily visible in CA1. Likewise, this procedure allowed for more direct comparisons of spike-phase relationships across subregions. As theta in CA1 is known to exhibit an asymmetric saw-toothed shape rather than a sinusoidal rhythm, we followed the protocol established by Belluscio et al. (2012) when defining the borders between phase components (e.g., peak, falling, trough, rising). In brief, phase centers, established as the peak, trough, and zero crossings of the LFP time series, are first found for a narrowly filtered theta band (6 -12 Hz). The LFP is then re-filtered in a broader band (3 - 20 Hz) and phase centers established from the narrow band are re-defined to be the closest peaks, troughs, and zero-crossings detected in the broader band.

Histology

After experiments were completed, a 20–40 μA current was passed through each recording tetrode for 20-40 s while rats were under anesthesia immediately prior to euthanizing the rat, with the resulting brain lesions serving as confirmation of tetrode position. Transcardial perfusions were performed with 0.9% saline followed by 4% formalin. Brains were extracted and allowed to sit for several days in 4% formalin solution. Brains were moved to a 40% sucrose solution for approximately 72 hours, until brains sank to the bottom of the container, at which point brains were sliced into approximately 70 μm coronal slices and mounted on glass microscope slides. Brains were left for several days to dry in an 37° C oven, then Nissl stained with a cresyl violet solution.

Supplemental References

Anderson, M. I., & O'Mara, S. M. (2003). Analysis of recordings of single-unit firing and population activity in the dorsal subiculum of unrestrained, freely moving rats. *Journal of Neurophysiology, 90*, 655-665.

Belluscio, M. A., Mizuseki, K., Schmidt, R., Kempter, R., & Buzsáki, G. (2012). Cross-frequency phase–phase coupling between theta and gamma oscillations in the hippocampus. *J. Neurosci., 32*, 423-435.

Bragin, A. N. A. T. O. L., Jando, G., Nadasdy, Z., Van Landeghem, M., & Buzsáki, G. (1995). Dentate EEG spikes and associated interneuronal population bursts in the hippocampal hilar region of the rat. *Journal of Neurophysiology, 73*, 1691-1705.

Buzsáki, G. (1986). Hippocampal sharp waves: their origin and significance. *Brain research, 398*, 242-252.

Delorme, A. & Makeig, S. (2004). EEGLAB: An open source toolbox for analysis of single-trial EEG dynamics. *J. Neurosci. Methods*, *134*, 9-21.

Delorme, A., Mullen, T., Kothe, C., Acar, Z.A., Bigdely-Shamlo, N., Vankov, A., & Makeig, S. (2011). EEGLAB, SIFT, NFT, BCILAB, and ERICA: New tools for advanced EEG processing. *Computational Intelligence and Neuroscience*, Article ID 130714.

Ding, M., Bressler, S. L., Yang, W., & Liang, H. (2000). Short-window spectral analysis of cortical event-related potentials by adaptive multivariate autoregressive modeling: data preprocessing, model validation, and variability assessment. *Biol. Cybern. 83*, 35-45.

Gaarskjaer, F. (1986). The organization and development of the hippocampal mossy fiber system. *Brain Res. Rev., 11*, 335-357.

Kaminski, M. J., & Blinowska, K. J. (1991). A new method of the description of the information flow in the brain structures. *Biol. Cybern., 65*, 203-210.

Maris, E., & Oostenveld, R. (2007). Nonparametric statistical testing of EEG-and MEG-data. *J. Neurosci.* Methods, *164*, 177-190.

Maris, E., Schoffelen, J-M., & Fries, P. (2007). Nonparametric statistical testing of coherence differences. *J. Neurosci. Methods, 163*, 161-175.

Mitra, P. P., & Pesaran, B. (1999). Analysis of dynamic brain imaging data. *Biophysical Journal, 76*(2), 691-708.

Mullen, T.R. (2014). The dynamic brain: Modeling neural dynamics and interactions from human electrophysiological recordings (Doctoral dissertation). Available from Dissertations & Theses at University of California; ProQuest Dissertations and Theses A&I. (UMI No. 1619637939)

Ranck, J. B. (1973). Studies on single neurons in dorsal hippocampal formation and septum in unrestrained rats: Part I. Behavioral correlates and firing repertoires. *Exp. Neurol. 41*, 462-531.

Skaggs, W. E., & McNaughton, B. L. (1996). Theta phase precession in hippocampal. *Hippocampus*, *6*, 149-172.

Swanson, L. W., Wyss, J. M., & Cowan, W. M. (1978). An autoradiographic study of the organization of intrahippocampal association pathways in the rat. *J. Comp. Neurol*., *181*, 681-715.

Witter, M. P., & Amaral, D. G. (2004). The hippocampal region. *The Rat Brain (Paxinos G, ed)*, 637-703.